

Rational Design of Fluorogenic and Spontaneously Blinking Labels for Super-Resolution Imaging

Qinsi Zheng,[†] Anthony X. Ayala,[†] Inhee Chung,^{†,||} Aubrey V. Weigel,[†] Anand Ranjan,[‡] Natalie Falco,[†] Jonathan B. Grimm,[†] Ariana N. Tkachuk,[†] Carl Wu,[‡] Jennifer Lippincott-Schwartz,[†] Robert H. Singer,^{†,§} and Luke D. Lavis^{*,†,§}

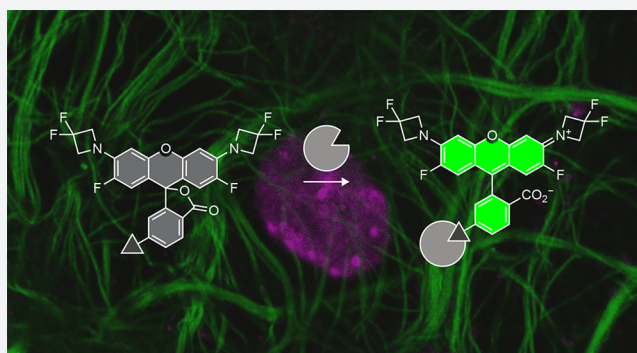
[†]Janelia Research Campus, Howard Hughes Medical Institute, Ashburn, Virginia 20147, United States

[‡]Department of Biology and Department of Molecular Biology and Genetics, Johns Hopkins University, Baltimore, Maryland 21218, United States

[§]Department of Anatomy and Structural Biology, Albert Einstein College of Medicine, Bronx, New York 10461, United States

S Supporting Information

ABSTRACT: Rhodamine dyes exist in equilibrium between a fluorescent zwitterion and a nonfluorescent lactone. Tuning this equilibrium toward the nonfluorescent lactone form can improve cell-permeability and allow creation of “fluorogenic” compounds—ligands that shift to the fluorescent zwitterion upon binding a biomolecular target. An archetype fluorogenic dye is the far-red tetramethyl-Si-rhodamine (SiR), which has been used to create exceptionally useful labels for advanced microscopy. Here, we develop a quantitative framework for the development of new fluorogenic dyes, determining that the lactone–zwitterion equilibrium constant (K_{L-Z}) is sufficient to predict fluorogenicity. This rubric emerged from our analysis of known fluorophores and yielded new fluorescent and fluorogenic labels with improved performance in cellular imaging experiments. We then designed a novel fluorophore—Janelia Fluor 526 (JF₅₂₆)—with SiR-like properties but shorter fluorescence excitation and emission wavelengths. JF₅₂₆ is a versatile scaffold for fluorogenic probes including ligands for self-labeling tags, stains for endogenous structures, and spontaneously blinking labels for super-resolution immunofluorescence. JF₅₂₆ constitutes a new label for advanced microscopy experiments, and our quantitative framework will enable the rational design of other fluorogenic probes for bioimaging.



INTRODUCTION

Small-molecule fluorophores are fundamental tools for biological research.^{1,2} The century-old^{3,4} rhodamine dyes remain the most useful class of small-molecule fluorophores and serve as scaffolds for a variety of useful imaging probes including biomolecule labels, cellular stains, and environmental indicators.^{5,6} This broad utility can be attributed to three key aspects of rhodamine dyes:^{7–20} (i) exceptional brightness and photostability; (ii) a broad palette of spectral properties accessed through straightforward structural modifications; and (iii) the equilibrium between the colorless, nonfluorescent lactone (L) and the colored, fluorescent zwitterion (Z; equilibrium constant: K_{L-Z}). Tuning K_{L-Z} lower—toward the lipophilic nonfluorescent lactone form—can improve cell-permeability²⁰ and yield “fluorogenic” ligands,^{14,16,20–24} molecules that show substantial increases in absorption and fluorescence upon binding their cognate biomolecular targets.

The inherent fluorescence increase of fluorogenic ligands is particularly useful for biological imaging as such compounds remain quiescent until bound to their target, making them universal platforms for imaging and sensing.²⁵ This property can

avoid the need to wash out excess ligand²⁰ and allow exchange of labels to circumvent photobleaching.²⁶ Many useful fluorogenic ligands exploit solvatochromism,^{27,28} pH sensitivity,^{29,30} photo-induced electron transfer (PeT),³¹ or quencher ejection³² to translate the binding event into a change in fluorescence intensity. Recently, the tetramethyl-Si-rhodamine (SiR, 1; Figure 1a) has emerged as a remarkably versatile fluorogenic dye, demonstrated first by Johnsson and co-workers.¹⁴ Compound 1 exhibits far-red wavelengths with an absorption maximum (λ_{abs}) of 643 nm, a fluorescence emission maximum (λ_{em}) of 662 nm, a modest fluorescence quantum yield ($\Phi = 0.41$, Table 1), and excellent photostability. An important feature of SiR-based ligands is the relatively low K_{L-Z} value (0.0034), which means the dye preferentially adopts the nonfluorescent lactone in aqueous solution (Figure 1a). This results in a lower extinction coefficient in aqueous solution ($\epsilon_w = 28\,200\text{ M}^{-1}\text{ cm}^{-1}$) but makes SiR-based ligands highly cell-permeable due to the increased fraction of the lipophilic lactone.

Received: July 9, 2019

Published: September 5, 2019

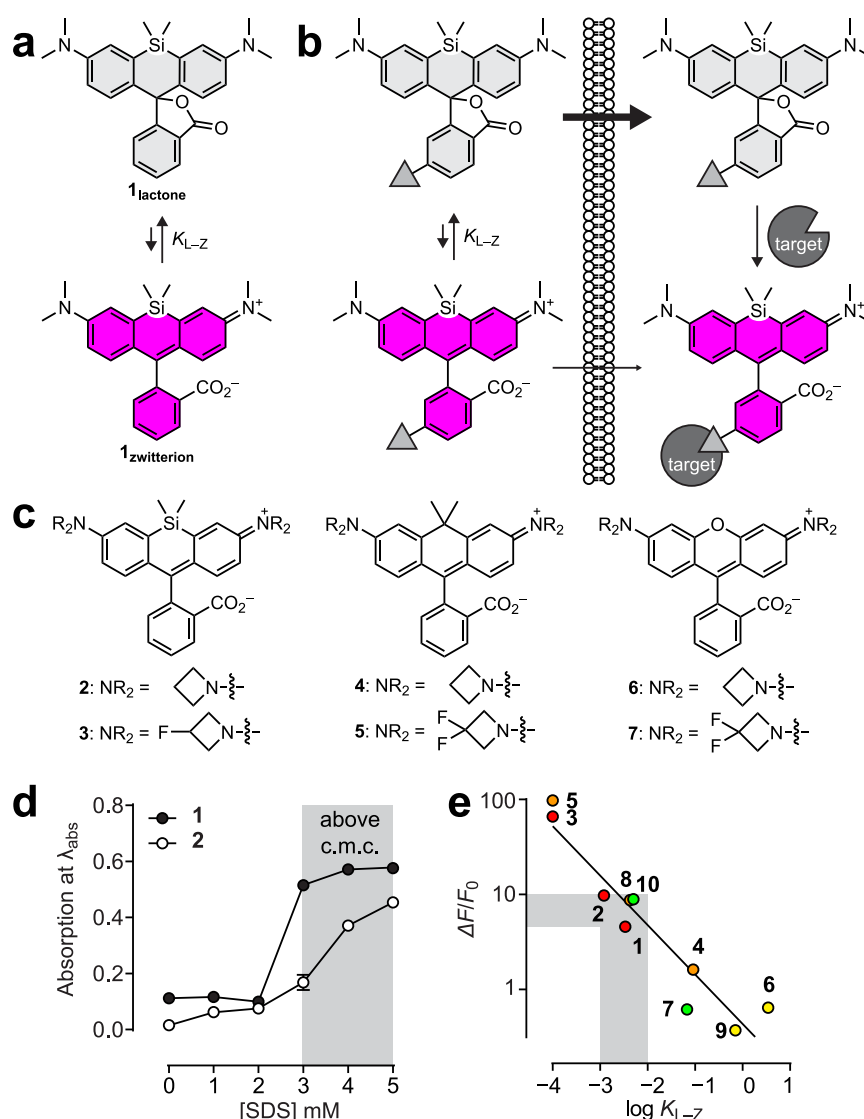


Figure 1. Fluorogenicity of rhodamines. (a) Lactone–zwitterion equilibrium of SiR (1). (b) Mechanism of improved cell-permeability and fluorogenicity of 1. (c) Structures of Janelia Fluor dyes 2–7. (d) Absorption at λ_{abs} vs SDS concentration for 1 and 2 in 20 mM Na_2HPO_4 , pH 7.0; error bars show \pm s.e.m.; shading indicates [SDS] above the critical micelle concentration (c.m.c.).³⁶ (e) Change in fluorescence over the basal fluorescence ($\Delta F/F_0$) of HaloTag ligands 1_{HTL}–10_{HTL} upon labeling purified HaloTag protein vs the K_{L-Z} of the corresponding free dyes 1–10; solid line indicates a linear fit ($R^2 = 0.90$); shading indicates $\Delta F/F_0 = 5-10$ and $K_{L-Z} = 10^{-2}-10^{-3}$.

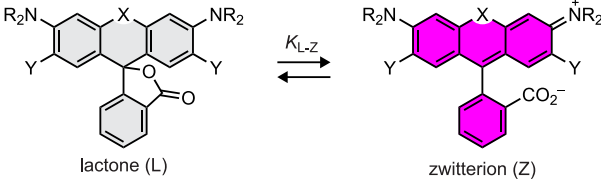
The lower K_{L-Z} also makes SiR compounds fluorogenic as binding to biomolecular targets often shifts the equilibrium toward the fluorescent zwitterionic form (Figure 1b).

The initial development of SiR-based labels focused on fluorogenic ligands for genetically encoded self-labeling tags like the HaloTag and the SNAP-tag¹⁴ but soon expanded to stains for endogenous structures like microtubules, F-actin, and DNA,^{22–24} as well as sensors for disparate analytes.^{12,33,34} The cell-permeability, brightness, photostability, and far-red wavelengths of SiR ligands have enabled advanced imaging experiments using structured illumination microscopy (SIM) and stimulated emission depletion (STED) imaging.¹⁴ The low K_{L-Z} of SiR also spurred the development of hydroxymethyl (HM) derivatives of SiR that spontaneously blink under physiological conditions and are useful for single-molecule localization microscopy (SMLM).³⁵ In another extension, our laboratory discovered that replacing the *N,N*-dimethylamino groups in fluorophores with four-membered azetidine rings was a general strategy to improve properties. Applying this strategy

to SiR yielded a brighter and more fluorogenic dye: “Janelia Fluor” 646 (JF₆₄₆; 2; $\lambda_{\text{abs}}/\lambda_{\text{em}} = 646 \text{ nm}/664 \text{ nm}$, $\epsilon_w = 5000 \text{ M}^{-1} \text{ cm}^{-1}$, $\Phi = 0.56$, $K_{L-Z} = 0.0012$).¹⁶ We could fine-tune this Si-rhodamine by incorporating 3-fluoroazetidine into the structure, yielding JF₆₃₅ (3, $\lambda_{\text{abs}}/\lambda_{\text{em}} = 635 \text{ nm}/652 \text{ nm}$, $\epsilon_w \approx 400 \text{ M}^{-1} \text{ cm}^{-1}$, $\Phi = 0.54$), which exhibited a low K_{L-Z} value (<0.0001) and high fluorogenicity. This universal approach could be applied to carborhodamine and standard oxygen-containing rhodamine scaffolds to yield bright fluorescent and fluorogenic dyes across the visible spectrum (4–7, Figure 1c, Table 1).^{16,20}

We set out to expand the palette of fluorogenic molecules with the goal of creating a green-emitting version of SiR. We first investigated the relationship between K_{L-Z} of dyes 1–7 and the fluorogenicity of their respective HaloTag ligands to determine a quantitative framework for the rational design of new fluorogenic rhodamine dyes. We discovered that the K_{L-Z} is sufficient to predict fluorogenicity, and we determined that $K_{L-Z} < 10^{-2}$ was an appropriate threshold for the design of highly fluorogenic ligands, validating this with the known Si-rhodamine

Table 1. Properties of Rhodamine Dyes



dye	X	Y	NR ₂	λ_{abs} (nm)	λ_{em} (nm)	ϵ_{w} (M ⁻¹ cm ⁻¹)	ϵ_{max} (M ⁻¹ cm ⁻¹)	Φ	$K_{\text{L-Z}}$
1	Si(CH ₃) ₂	H		643	662	28,200	141,000	0.41	0.0034
2	Si(CH ₃) ₂	H		646	664	5,000	152,000	0.54	0.0012
3	Si(CH ₃) ₂	H		635	652	~400	167,000	0.56	<0.0001
4	C(CH ₃) ₂	H		608	631	99,000	121,000	0.67	0.091
5	C(CH ₃) ₂	H		585	609	1,500	156,000	0.78	<0.0001
6	O	H		549	571	101,000	134,000	0.88	3.5
7	O	H		525	549	94,000	122,000	0.91	0.068
8	Si(CH ₃) ₂	H		587	609	2,200	94,000	0.53	0.0043
9	O	F		552	575	95,000	129,000	0.83	0.70
10	O	F		526	550	19,000	118,000	0.87	0.0050

110 (SiR₁₁₀, **8**). We next turned to the oxygen-containing rhodamine scaffold, first preparing derivatives of a tuned dye, JF₅₅₂ (**9**), and then the rationally designed fluorophore JF₅₂₆ (**10**). This dye shows similar fluorogenicity to SiR, allows the creation of fluorogenic labels and stains, and can be further modified to a spontaneously blinking derivative that enables facile localization microscopy in cells.

RESULTS AND DISCUSSION

Mechanism of SiR/JF₆₄₆ Fluorogenicity. In previous studies, the fluorogenicity of ligands based on SiR and other rhodamines was attributed, in part, to the formation of weakly fluorescent aggregates.^{14,37} The key evidence for this mechanism was the large increase in absorption that occurred when the detergent sodium dodecyl sulfate (SDS) was added to aqueous solutions of SiR-based compounds, presumably disaggregating the dye. We investigated this phenomenon and found it was detergent-specific; incubation of SiR (**1**) and JF₆₄₆ (**2**) with commonly used laboratory detergents showed absorption increases only in the presence of SDS (Figure S1a). We further characterized the interaction between the Si-rhodamine dyes **1** and **2** and SDS by measuring the absorption of **1** or **2** versus [SDS] and observed the absorption increase only above the critical micelle concentration (c.m.c.) of SDS (Figure 1d). These results suggest another mechanism for this observed increase in absorption, where dyes **1** and **2** interact with the negatively charged SDS-micelle surface, thereby stabilizing the zwitterionic form and giving the observed increase in absorption. This is further supported by the bathochromic shift in λ_{abs} observed for **1** and **2** in the presence of SDS (Figure S1b,c), which is characteristic for rhodamine–SDS-micelle complexes.³⁸ These data reveal a problem with the use of SDS solutions to determine

the spectral properties of fluorogenic dyes as the measurement is strongly concentration- and dye-dependent (Figure 1d). We instead use a solution of strong acid in alcohol solvents to shift the equilibrium to the open form by protonation of the *o*-carboxyl group. This decades-old procedure^{39,40} allows estimation of the maximal extinction coefficient (ϵ_{max}) and determination of $K_{\text{L-Z}}$ (Supporting Information).

On the basis of these results, we hypothesized that the low $K_{\text{L-Z}}$ value was the primary driver behind the fluorogenicity of SiR and similar fluorogenic rhodamines. In this mechanism, the fluorophores preferentially adopt the colorless lactone form in solution, largely independent of concentration, dye structure, or ligand moiety. Binding to the biomolecule shifts the equilibrium to the fluorescent zwitterionic form through steric interactions and other changes to the local chemical environment. Aggregation of such compounds can still occur, particularly for high concentrations of dyes that prefer the lipophilic lactone form, but this is a consequence of the low $K_{\text{L-Z}}$ and not the causal element behind the observed fluorogenicity. To test this premise, we examined the relationship between $K_{\text{L-Z}}$ for a series of fluorescent dyes (**1–7**, Figure 1c, Table 1) and the increase in fluorescence of the corresponding HaloTag ligands upon conjugation to purified HaloTag protein (**1_{HTL}–7_{HTL}**, Figure 1e, Figure S1d). The $K_{\text{L-Z}}$ was determined using ϵ values measured in 1:1 dioxane:water (ϵ_{dw}) to ensure a broad distribution of values.²⁰ We found an inverse relationship between $K_{\text{L-Z}}$ and fluorogenicity, showing that $K_{\text{L-Z}}$ is sufficient to predict the increase in fluorescence of different rhodamine dyes upon binding the same target. This increase in fluorescence is primarily driven by a rise in absorption; chromogenicity is correlated with both $K_{\text{L-Z}}$ and fluorogenicity (Figure S1e,f). This trend holds across different rhodamine scaffolds including

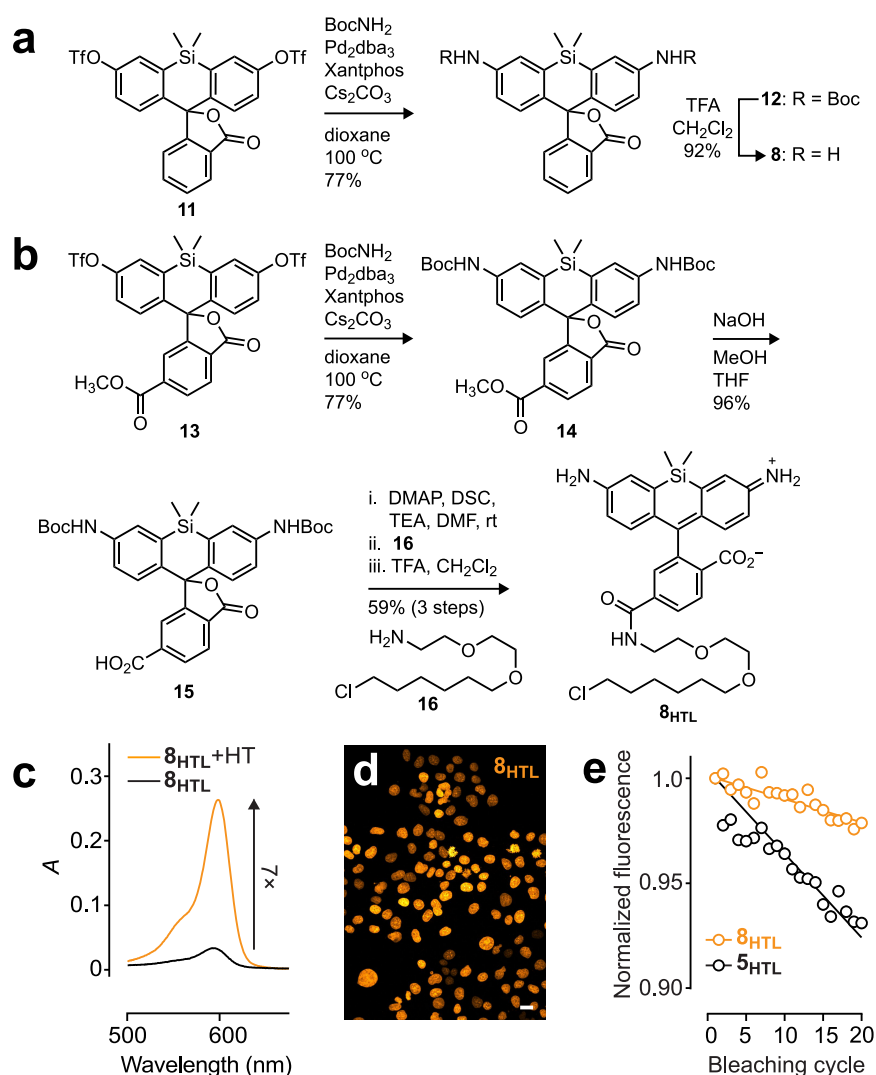


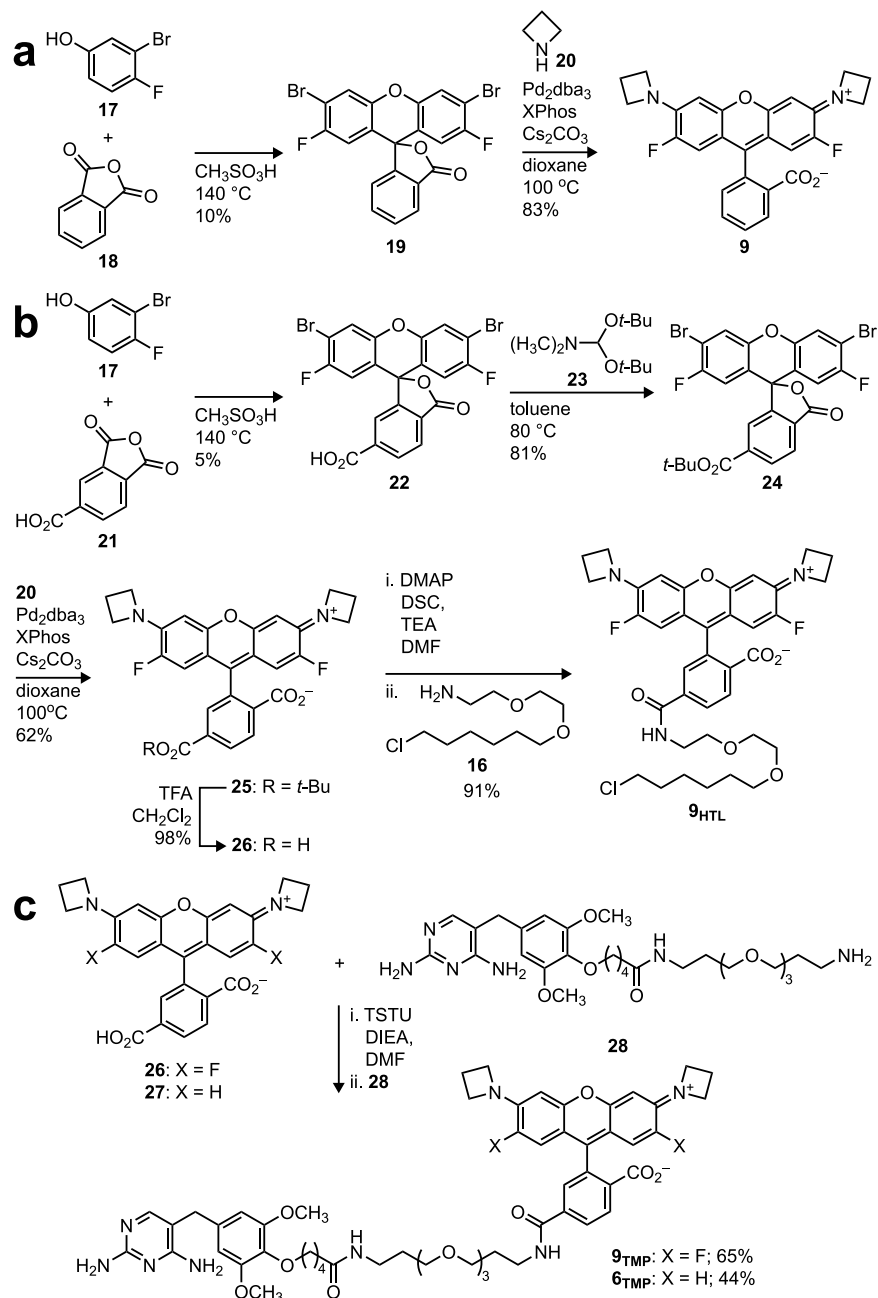
Figure 2. Synthesis and testing of SiR₁₁₀. (a) Synthesis of SiR₁₁₀ (**8**). (b) Synthesis of SiR₁₁₀-HaloTag ligand (**8_{HTL}**). (c) Absorption spectra of **8_{HTL}** (5 μM) in the absence (black) or presence (orange) of excess HaloTag protein. (d) Confocal image of U2OS cells expressing histone H2B-8_{HTL} fusion protein and labeled with **8_{HTL}**. Scale bar: 20 μm. (e) Relative photostability of **8_{HTL}** and JF₅₈₅-HaloTag ligand (**5_{HTL}**) in live cells.

Si-rhodamines (**1–3**), carborhodamines (**4** and **5**), and classic, oxygen-containing rhodamines (**6** and **7**, Figure 1c). This inverse relationship yielded a simple rubric: a dye with $K_{L-Z} = 10^{-2}$ – 10^{-3} should yield a HaloTag ligand with 5–10-fold fluorogenicity (Figure 1e).

Si-Rhodamine 110. In previous work, we developed strategies to fine-tune the properties of rhodamines by incorporating substituted azetidines into the dye structure.²⁰ In particular, we developed the bright, fluorogenic carborhodamine JF₅₈₅ (**5**, Figure 1c; $\lambda_{\text{abs}}/\lambda_{\text{em}} = 585 \text{ nm}/609 \text{ nm}$, $\Phi = 0.78$) by replacing the azetidine rings in JF₆₀₈ (**4**; $\lambda_{\text{abs}}/\lambda_{\text{em}} = 608 \text{ nm}/631 \text{ nm}$, $\Phi = 0.67$) with 3,3-difluoroazetidine; the K_{L-Z} -fluorogenicity trend holds for these dyes (Figure 1e). As an alternative strategy to create orange-emitting fluorogenic dyes, we investigated the Si-containing analogue of rhodamine 110 (**8**), which has been described as a scaffold for fluorogenic enzyme substrates in the patent literature⁴¹ but has not been used as a fluorescent label in cellular experiments. We synthesized this compound using the Pd-catalyzed cross-coupling of the Si-fluorescein ditriflate (**11**) with *t*-butyl carbamate followed by deprotection with TFA (Figure 2a).^{16,42} Compound **8** exhibited $\lambda_{\text{max}}/\lambda_{\text{em}} = 587 \text{ nm}/609 \text{ nm}$,

representing a ~50 nm hypsochromic shift relative to SiR (**1**; $\lambda_{\text{abs}}/\lambda_{\text{em}} = 643 \text{ nm}/662 \text{ nm}$, Table 1); we named this dye Si-rhodamine 110 (SiR₁₁₀). It has an increased fluorescence quantum yield ($\Phi = 0.53$) compared to SiR ($\Phi = 0.41$, Table 1), but a comparable $K_{L-Z} = 0.0043$.

On the basis of our K_{L-Z} versus fluorogenicity relationship (Figure 1e), we predicted that ligands based on **8** would be fluorogenic. This was a noteworthy test of our hypothesis since SiR₁₁₀ has similar K_{L-Z} values to SiR but a different structure—lacking the four hydrophobic CH₃ groups in **1**. We prepared the SiR₁₁₀-HaloTag ligand (**8_{HTL}**, Figure 2b) starting from the 6-carboxy-Si-fluorescein ditriflate methyl ester (**13**).⁴³ Cross-coupling afforded the Boc-protected SiR₁₁₀ **14**, which was saponified to yield free acid **15**. Formation of the *N*-hydroxysuccinimidyl ester *in situ*, amidation with the HaloTag ligand (**16**), and deprotection with TFA yielded **8_{HTL}**. We observed a 7-fold increase in absorption and $\Delta F/F_0 = 9$ after conjugation of **8_{HTL}** to HaloTag protein, slightly higher than SiR-HaloTag ligand (**1_{HTL}**; $\Delta F/F_0 = 5$; Figure 2c, Figure S1d) and in line with the K_{L-Z} trend (Figure 1e). This dye was an excellent label for live-cell imaging experiments (Figure 2d) and showed higher photostability than our previously described

Scheme 1. Syntheses of JF₅₅₂ and JF₅₄₉ Derivatives: (a) Synthesis of **9**, (b) Synthesis of **9_{HTL}**, and (c) Synthesis of **6_{TMP}** and **9_{TMP}**

orange-emitting fluorogenic JF₅₈₅–HaloTag ligand (**5_{HTL}**, Figure 2e). These results further support our hypothesis that a low K_{L-Z} value is a primary factor for rhodamine fluorogenicity.

Janelia Fluor 552. We then turned to the standard, oxygen-containing rhodamine scaffold exemplified by JF₅₄₉ (**6**, Figure 1c; $\lambda_{abs}/\lambda_{em}$ = 549 nm/571 nm, Φ = 0.88). Creating a fluorogenic rhodamine is challenging since this dye type strongly prefers the fluorescent zwitterionic form; JF₅₄₉ exhibits a high K_{L-Z} = 3.5, which is $>10^2$ -fold higher than the apparent K_{L-Z} threshold for a fluorogenic ligand (Figure 1e). Incorporation of 3,3-difluoroazetidine motifs into the JF₅₄₉ structure yields JF₅₂₅ (**7**), which shows a lower K_{L-Z} = 0.068 and elicits ~ 25 nm hypsochromic shift with similar brightness ($\lambda_{max}/\lambda_{em}$ = 525 nm/549 nm, Φ = 0.91; Table 1). This K_{L-Z} tuning is insufficient to achieve substantial fluorogenicity although the JF₅₂₅–HaloTag ligand (**7_{HTL}**) exhibits higher cell-permeability

than the JF₅₄₉–HaloTag ligand (**6_{HTL}**)²⁰ and can cross the blood–brain barrier.⁴⁴ Since we exhausted the available substitutions on the azetidine ring with JF₅₂₅, we sought a complementary approach for further modulating K_{L-Z} . We recently reported a JF₅₄₉ analogue with fluorine atoms installed at the 2' and 7' positions on the xanthene ring. This modification reduced the K_{L-Z} by 5-fold (K_{L-Z} = 0.70) with only a minor shift in spectral properties ($\lambda_{abs}/\lambda_{em}$ = 552 nm/575 nm, Φ = 0.83; Table 1).¹⁹ The resulting dye, Janelia Fluor 552 (JF₅₅₂; **9**), is of particular interest because it could show improved cell-permeability relative to JF₅₄₉ and could be further modified to create a fluorogenic rhodamine.

We aimed to develop a general synthetic strategy for JF₅₅₂ derivatives that would also allow late-stage incorporation of different azetidiny functionality. Unfortunately, our standard Pd-catalyzed cross-coupling approach for rhodamines^{42,45} gave

low yield (<5%) when starting with 2',7'-difluorofluorescein ditriflate due to the instability of the *o*-fluorophenyl triflate groups (data not shown). To circumvent this problem, we devised an alternative synthesis starting with 3-bromo-4-fluorophenol (**17**, Scheme 1a). Acid-mediated condensation of **17** and phthalic anhydride (**18**) yielded dibromofluoran **19**. Pd-catalyzed cross-coupling with azetidine (**20**) provided JF₅₅₂ (**9**). To introduce a carboxyl group for bioconjugation, we condensed phenol **17** and with trimellitic anhydride (**21**) to give an isomeric mixture; crystallization from 9:1 toluene:pyridine yielded the 6-carboxy isomer **22**. This was protected as the *t*-butyl ester using *N,N*-dimethylformamide di-*t*-butyl acetal (**23**) to yield **24**, followed by Pd-catalyzed cross-coupling with azetidine (**20**) to provide 6-carboxy-JF₅₅₂ *t*-butyl ester (**25**). Deprotection of **25** with TFA yielded carboxylic acid **26**, and subsequent conjugation to the HaloTag ligand amine (**16**) gave JF₅₅₂-HaloTag ligand **9**_{HTL} (Scheme 1b). On the basis of these results, we briefly attempted to transform 2',7'-difluorofluorescein ditriflates to their respective dibromofluorans using Ru catalysts.⁴⁶ This reaction was successful for the synthesis of dibromide **19** but gave poor yields of *t*-butyl ester **24** (data not shown).

We then evaluated JF₅₅₂ ligands as cell-permeable fluorescent labels, comparing the JF₅₅₂-HaloTag ligand (**9**_{HTL}) to JF₅₄₉-HaloTag ligand (**6**_{HTL}, Figure S1d) in yeast expressing histone H2A.Z-HaloTag protein fusion. Although **6**_{HTL} showed relatively poor labeling (Figure 3a), the **9**_{HTL} molecule showed

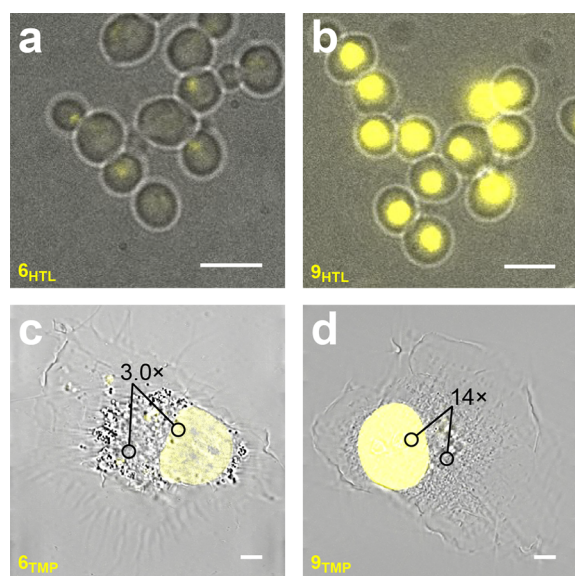


Figure 3. JF₅₅₂ ligands show improved cell-permeability. Overlay of fluorescence and bright-field images of yeast cells expressing a histone H2A.Z-HaloTag fusion protein and labeled with **6**_{HTL} (a) or **9**_{HTL} (b). Overlay of fluorescence and bright-field images of U2OS cells expressing histone H2B-eDHFR fusion protein and labeled with **6**_{TMP} (c) or **9**_{HTL} (d). Scale bars for all images: 5 μ m.

a high fluorescence signal from the yeast nuclei under the same imaging conditions (Figure 3b). This result is expected on the basis of the smaller K_{L-Z} of JF₅₅₂, which should improve cell-permeability. We also synthesized the trimethoprim (TMP) conjugates of JF₅₄₉ and JF₅₅₂ (**6**_{TMP} and **9**_{TMP}) by reacting the 6-carboxy derivatives of these dyes (**26** and **27**, respectively) with the amino-TMP **28** (Scheme 1c). TMP conjugates selectively bind to *Escherichia coli* dihydrofolate reductase (eDHFR), and

this labeling strategy can be used for live-cell imaging.⁴⁷ We expressed histone H2B-eDHFR fusions in U2OS cells and labeled with **6**_{TMP} or **9**_{TMP}. Nuclei labeled with JF₅₅₂-based **9**_{TMP} were 8-fold brighter than cells labeled with **6**_{TMP}, giving images with higher signal-to-background (Figure 3c,d). These results support our hypothesis that even modest decreases in K_{L-Z} can improve cell-permeability across different cell-types and labeling strategies.

Janelia Fluor 526. We then combined the structural modifications of **7** (K_{L-Z} = 0.068) and **9** (K_{L-Z} = 0.70), positing that the two complementary alterations could additively shift the K_{L-Z} < 10^{-2} , thus yielding a fluorogenic rhodamine. To prepare the free dye we used Pd-catalyzed cross-coupling to attach 3,3-difluoroazetidine (**29**) to dibromide **19** yielding the hexafluorinated rhodamine **10** (Figure 4a). We termed the resulting compound Janelia Fluor 526 (JF₅₂₆; $\lambda_{abs}/\lambda_{em}$ = 526 nm/550 nm, Φ = 0.87), which exhibited the desired additive effect on the lactone-zwitterion equilibrium (K_{L-Z} = 0.0050; Table 1). We then synthesized the 6-carboxy derivative using a route akin to the JF₅₅₂ ligands (Scheme 1b): cross-coupling of dibromide **24** with azetidine **29** to give *t*-butyl ester **30** followed by deprotection with TFA to give **31**. This compound could be coupled to amine-containing ligand moieties to yield JF₅₂₆-HaloTag ligand (**10**_{HTL}) and JF₅₂₆-SNAP-tag ligand (**10**_{STL}, Figure 4b, Scheme S1a). We compared this with the previously described JF₅₂₅-HaloTag ligand²⁰ (**7**_{HTL}) *in vitro* and in live cells. Although **7**_{HTL} exhibited a modest <2-fold increase of absorption upon conjugation to purified HaloTag protein, **10**_{HTL} exhibited a substantial 9-fold increase (Figure S2a,b), again following the K_{L-Z} -fluorogenicity trend (Figure 1e). JF₅₂₆ showed superior signal-to-background compared to JF₅₂₅ in “no-wash”, live-cell imaging experiments using either the HaloTag (Figure 4d,e) or SNAP-tag expressed as histone H2B fusion proteins (**10**_{STL} versus **7**_{STL}, Figure 4f,g).

We then prepared other JF₅₂₆ ligands (Figure 4b, Scheme S1b-d) to demonstrate the general utility of this dye for multicolor advanced microscopy experiments. On the basis of previous work with SiR (**1**), JF₆₄₆ (**2**), and other dyes,^{22–24,48,49} we synthesized the following conjugates: JF₅₂₆-Hoechst (**10**_{HST}) to stain DNA, JF₅₂₆-Taxol (**10**_{TXL}) to image microtubules, and JF₅₂₆-pepstatin A (**10**_{PEP}) to visualize lysosomes (Figures 4b and 5a). **10**_{HST} showed a modest increase in absorption (<2-fold) and a large increase in fluorescence quantum yield (10-fold) upon binding purified AT-rich DNA (Figure S2c,d), showing that chromogenicity can be magnified by other photophysical effects. The JF₅₂₆-Taxol (**10**_{TXL}) also showed increased fluorescence upon binding to polymerized tubulin *in vitro*; this fluorogenicity was comparable to that of “SiR-tubulin” (**1**_{TXL})²² and higher than JF₅₂₅-Taxol (**7**_{TXL}; Figure S2e–h and Scheme S1e). Live-cell imaging with these compounds showed specific staining, enabling one-, two-, and three-color no-wash imaging experiments (Figure 5b–d). We then used JF₅₂₆ ligands in advanced microscopy. We performed two-color 3D-SIM⁵⁰ in live cells using JF₅₂₆-pepstatin A (**10**_{PEP}) and JF₆₄₆-Hoechst⁴⁹ (**2**_{HST}, Figure 6a). JF₅₂₆ also enabled multicolor super-resolution STED microscopy⁵¹ of microtubules using **10**_{TXL} depleted with 775 nm (Figure 6b, Figure S2i–k). Notably, the compatibility of JF₅₂₆ with the standard 775 nm depletion line facilitated three-color live-cell STED imaging using JF₅₂₆-Taxol (**10**_{TXL}, microtubules), JF₆₄₆-SNAP-tag ligand (**2**_{STL}) targeted to Sec61 β (endoplasmic reticulum), and JF₅₈₅-HaloTag ligand (**5**_{HTL}) targeted to TOMM20 (mitochondria, Figure 6c). Finally, the JF₅₂₆-

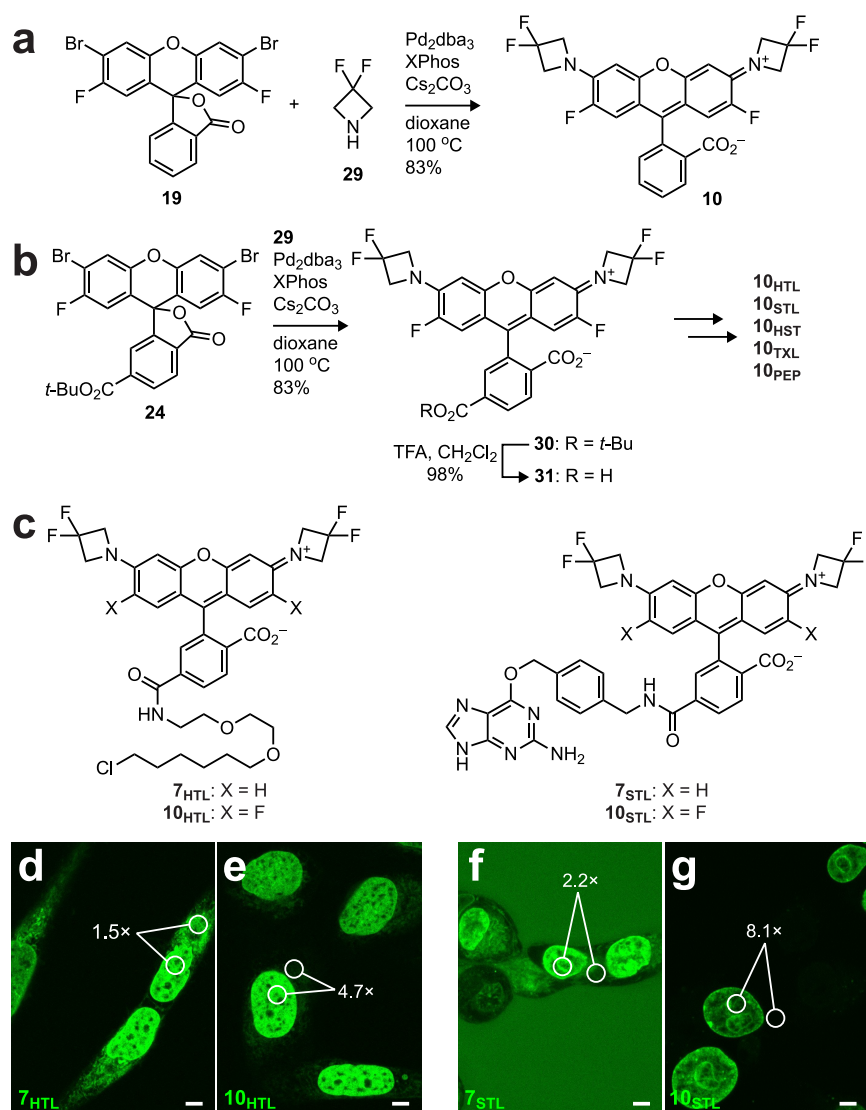


Figure 4. Synthesis and no-wash imaging of JF₅₂₆ ligands. Synthesis of JF₅₂₆ (a) and JF₅₂₆ (b) ligands. (c) Structures of JF₅₂₅ and JF₅₂₆–HaloTag and SNAP-tag ligands. Confocal images of COS7 cells expressing a histone H2B–HaloTag fusion protein and labeled with 500 nM JF₅₂₅–HaloTag ligand (7_{HTL}, d) or JF₅₂₆–HaloTag ligand (10_{HTL}, e). Confocal images of COS7 cells expressing histone H2B–SNAP-tag fusion protein and labeled with 1 μM JF₅₂₅–SNAP-tag ligand (7_{STL}, f) or JF₅₂₆–SNAP-tag ligand (10_{STL}, g). Scale bars for all images: 5 μm.

pepstatin A (10_{PEP}) could be used for live-cell, two-color lattice light-sheet microscopy⁵² with 2_{HST} (Figure 6d).

Hydroxymethyl JF₅₂₆. The lactone–zwitterion equilibrium of rhodamine dyes can be further exploited for single-molecule localization microscopy (SMLM). Converting the *o*-carboxyl moiety in SiR to the more nucleophilic hydroxymethyl group elicits an additional shift to the closed form.^{35,53} The resulting hydroxymethyl-SiR (HM-SiR, 32) exists primarily in a colorless, nonfluorescent spiroether form but spontaneously switches to a transient, fluorescent form upon protonation at physiological pH (Figure 7a). This blinking behavior enables facile SMLM imaging, bypassing the need for photoconvertible fluorescent proteins, photoactivatable dyes, or strongly reducing *d*STORM buffers.⁵⁴

Given the similarity of the K_{L-Z} values for JF₅₂₆ and SiR, we were curious if a hydroxymethyl derivative of JF₅₂₆ would show comparable utility to 32 in SMLM. We devised an efficient, high-yielding approach to synthesize derivatives of hydroxymethyl JF₅₂₆ (HM-JF₅₂₆), leveraging our divergent synthesis of JF₅₂₆ and the differential reactivity of carboxyl groups and lactones with

borohydride reductants.⁵⁵ Treatment of dibromofluoran 22 with LiBH₄ at ambient temperature selectively reduced the lactone to a cyclic ether leaving the 6-carboxy group intact, providing 33 in moderate yield (54%; Figure 7b). Formation of 6-*t*-butyl ester with acetal 23 gave 34, allowing Pd-catalyzed cross-coupling with 29. The resulting 6-*tert*-butoxycarbonyl-HM-JF₅₂₆ (35) can be deprotected to yield carboxylic acid 36 and then converted to amine-reactive *N*-hydroxysuccinimidyl ester 37 (HM-JF₅₂₆ NHS).

To evaluate the performance of HM-JF₅₂₆ in SMLM experiments we used 37 to label a goat-antimouse secondary antibody, followed by immunostaining of an anti-β-tubulin primary antibody in fixed cells. SMLM imaging in standard phosphate-buffered saline (pH 7.4) revealed that the HM-JF₅₂₆ label showed spontaneous blinking behavior throughout the imaging session and did not require short-wavelength activation light (Movie S1). Standard SMLM analysis transformed these movies into super-resolution images (Figure 7c,d); the HM-JF₅₂₆ label yielded 571 photons on average with a localization accuracy (σ) of 25 nm. The SMLM images showed fine

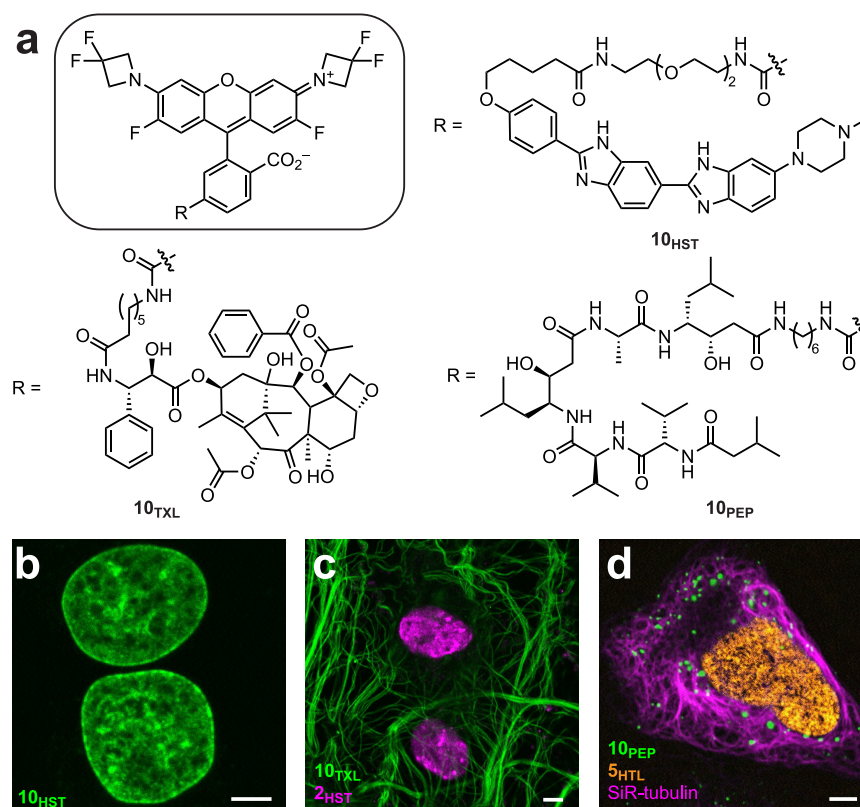


Figure 5. Extending the repertoire of JF₅₂₆ ligands. (a) Structures of JF₅₂₆ ligands. (b) Confocal image of live U2OS cells stained with JF₅₂₆–Hoechst (10_{HST}). (c) Confocal image of mouse primary hippocampal neurons stained with JF₅₂₆–Taxol (10_{TXL}) and JF₆₄₆–Hoechst (2_{HST}). (d) Confocal image of U2OS cells expressing histone-H2B–HaloTag fusion protein and labeled with JF₅₂₆–pepstatin A (10_{PEP}), JF₅₈₅–HaloTag ligand (5_{HTL}), and “SiR–tubulin” (1_{TXL}). All images were acquired without washing. Scale bars: 5 μ m.

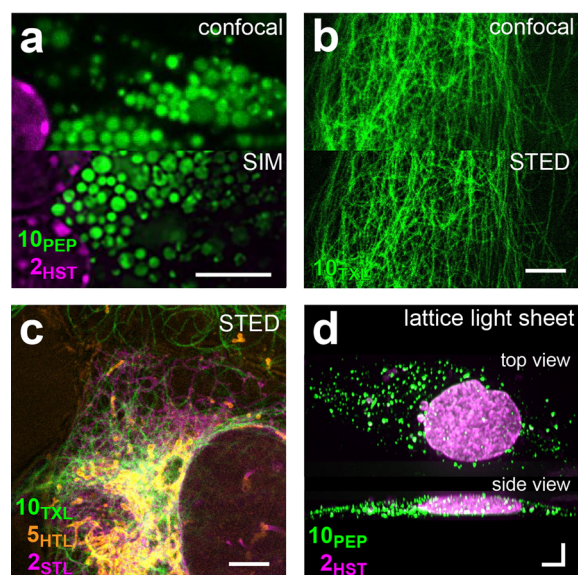


Figure 6. Advanced microscopy imaging using JF₅₂₆. (a) Confocal and SIM images of mouse primary hippocampal neurons stained with 10_{PEP} and JF₆₄₆–Hoechst (2_{HST}). (b) Confocal and STED microscopy images of U2OS cells stained with 10_{TXL}. (c) Three-color live-cell STED image of U2OS cells expressing Sec61 β –SNAP-tag labeled with JF₆₄₆–SNAP-tag ligand (2_{STL}), TOMM20–HaloTag labeled with JF₅₈₅–HaloTag ligand (5_{HTL}), and microtubules stained with 10_{TXL}. (d) Lattice light-sheet microscopy image of U2OS cells stained with 10_{PEP} and 2_{HST}. Scale bars for all images: 5 μ m.

structures of microtubules with a full width at half-maximum (fwhm) of 86 nm; diffraction-limited images had an fwhm of 253 nm (Figure 7e). We also labeled mitochondria using an anti-TOMM20 primary antibody which gave SMLM images of mitochondria with improved resolution (fwhm = 143 nm) compared to diffraction-limited images (fwhm = 581 nm; Figure 7f–h). HM-JF₅₂₆ constitutes a new label for SMLM that is spectrally distinct from HM-SiR and compatible with standard immunolabeling protocols.

CONCLUSION

Rhodamine dyes exist in equilibrium between a lipophilic, colorless lactone and a polar, fluorescent zwitterion. This property dictates many properties of rhodamines including cell-permeability and fluorogenicity. On the basis of the prototypical fluorogenic dye SiR (1) and the Janelia Fluor dyes (2–7), we showed that the equilibrium constant, K_{L-Z} , is sufficient to predict fluorogenicity by comparing the K_{L-Z} of rhodamines and the change in fluorescence of their respective HaloTag ligands upon binding their protein target. We found an inverse relationship between these two parameters and developed a quantitative framework for developing new fluorogenic molecules: tuning K_{L-Z} between 10^{-2} and 10^{-3} gives ligands with fluorogenicity of 5–10-fold (Figure 1). This rubric was validated with the orange-emitting dye, SiR₁₁₀ (8), which is fluorogenic and shows improved photostability compared to our previously described JF₅₈₅ (5, Figure 2).

Our previous attempts to tune the K_{L-Z} of standard rhodamine dyes using 3,3-difluoroazetidine substituents transformed JF₅₄₉ (6, K_{L-Z} = 3.5) to the highly bioavailable JF₅₂₅ (7,

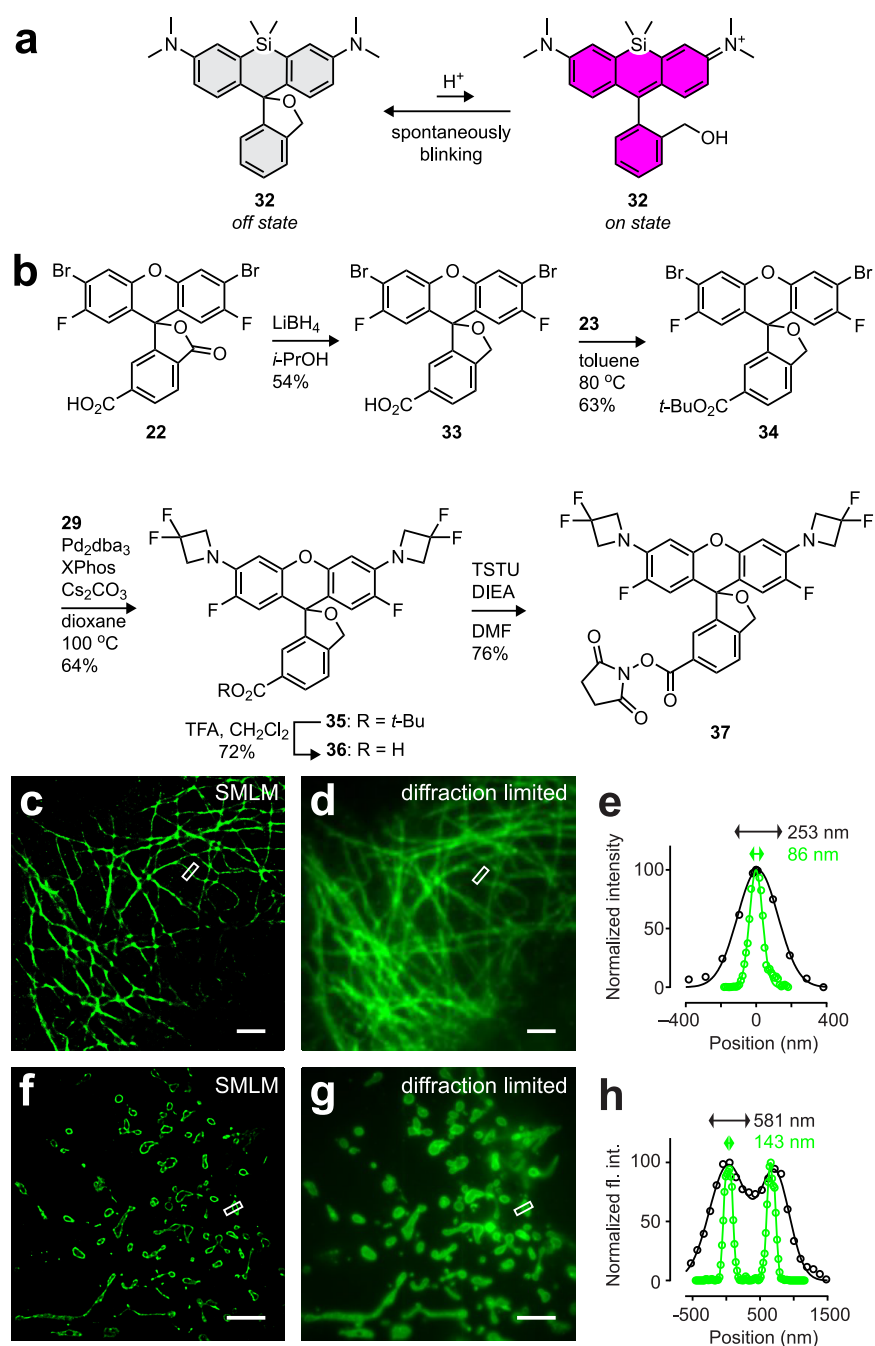


Figure 7. Localization microscopy with HM-JF₅₂₆. (a) Blinking behavior of HM-SiR (32). (b) Synthesis of HM-JF₅₂₆ NHS (37). Immunofluorescence images of tubulin labeled with a 37–antibody conjugate: (c) SMLM image, (d) diffraction-limited image. (e) Transverse profiles of fluorescence intensity corresponding to boxed regions in parts c and d. Immunofluorescence images of TOMM20 labeled with a 37–antibody conjugate: (f) SMLM image; (g) diffraction-limited image. (h) Transverse profiles of fluorescence intensity corresponding to boxed regions in parts f and g. Solid lines in parts e and h indicate Gaussian fits; numbers indicate the full width at half-maximum (fwhm) determined by the Gaussian fits of the SMLM (green) and diffraction-limited imaging (black). Scale bars for all images: 5 μm .

$K_{L-Z} = 0.068$). Nevertheless, this decrease in K_{L-Z} was insufficient to meet the fluorogenic threshold of $K_{L-Z} < 10^{-2}$; ligands based on JF₅₂₅ show low degrees of fluorogenicity. We used a complementary approach to further tune the K_{L-Z} by fluorinating the xanthene system. This yielded the highly cell-permeant JF₅₅₂ (9) as an intermediary product (Scheme 1, Figure 3) and ultimately led to the fluorogenic rhodamine JF₅₂₆ (10). Akin to SiR (1), JF₅₂₆ is a versatile scaffold for fluorogenic ligands, including labels for genetically encoded self-labeling protein tags (Figure 4) and stains for endogenous structures

(Figure 5). These green-emitting ligands can be used in concert with red- and orange-emitting fluorogenic dyes,^{14,16,20} allowing multicolor SIM and STED imaging in live cells (Figure 6). We further extended the utility of JF₅₂₆ to SMLM by creating the spontaneously blinking derivative: HM-JF₅₂₆ (Figure 7).

Looking forward, our results demonstrate the importance of K_{L-Z} in the rational design of fluorogenic and spontaneously blinking rhodamines, regardless of the specific dye structure. This general rubric we uncovered should enable rational design of fluorogenic and spontaneously blinking dyes using other

rhodamine variants, especially the exciting near-infrared derivatives containing phosphinate, phosphine oxide, or sulfone groups,^{15,17,18} pushing advanced microscopy to longer wavelengths. This quantitative approach could be applied to fluoresceins and rhodols, which bear *o*-carboxy groups and have environmentally sensitive equilibria between fluorescent and nonfluorescent lactone forms.^{13,19,56–58} Finally, we posit that the environmental sensitivity of fluorogenic rhodamines can be exploited beyond preparing ligands for no-wash imaging experiments. Like other fluorogenic molecules,^{59–61} transduction of protein conformational changes into fluorescence modulations will provide new hybrid small-molecule:protein sensors for functional imaging inside living cells and organisms.

Safety Statement. No unexpected or unusually high safety hazards were encountered.

■ ASSOCIATED CONTENT

Supporting Information

The Supporting Information is available free of charge on the ACS Publications website at DOI: [10.1021/acscentsci.9b00676](https://doi.org/10.1021/acscentsci.9b00676).

Methods for chemical synthesis, optical spectroscopy, and microscopy; and characterization data for all new compounds (PDF)

Movie S1: Time-lapse video of tubulin in fixed U2OS cells immunostained with HM-JF526 and excited with 561 nm laser light; no photoactivation laser was used; scale bar: 5 μ m (AVI)

■ AUTHOR INFORMATION

Corresponding Author

*E-mail: lavisl@janelia.hhmi.org.

ORCID

Jonathan B. Grimm: 0000-0003-0331-4200

Luke D. Lavis: 0000-0002-0789-6343

Present Address

[†]I.C.: Department of Anatomy and Cell Biology, George Washington University School of Medicine and Health Sciences, Washington, DC, USA.

Notes

The authors declare the following competing financial interest(s): L.D.L. and J.B.G. have filed patents and patent applications involving azetidine-containing dyes, whose value might be affected by this publication.

■ ACKNOWLEDGMENTS

We thank C. Deo and H. Bhargava for purified HaloTag protein, M. Freeman for cell culture, and D. Alcor for imaging technical (all at Janelia). We also thank J. M. Kim (Johns Hopkins) for assistance with yeast imaging. This work was supported by the Howard Hughes Medical Institute (Q.Z., J.B.G., I.C., A.V.W., A.X.A., A.N.T., J.L.-S., R.H.S., and L.D.L.) and NIH (A.R. and C.W.). The salary for R.H.S. is funded by NIH Grants NS083085 and EB021236.

■ REFERENCES

- (1) Lavis, L. D.; Raines, R. T. Bright ideas for chemical biology. *ACS Chem. Biol.* **2008**, *3*, 142–155.
- (2) Lavis, L. D.; Raines, R. T. Bright building blocks for chemical biology. *ACS Chem. Biol.* **2014**, *9*, 855–866.
- (3) Ceresole, M. *Verfahren zur Darstellung von Farbstoffen aus der Gruppe des Meta-amidophenolphthaleins*. German Patent 44002, 1887.

- (4) Ceresole, M. Production of new red coloring matter. U.S. Patent 377,349, 1888.

- (5) Haugland, R. P.; Spence, M. T. Z.; Johnson, I. D.; Bases, A. *The handbook: A guide to fluorescent probes and labeling technologies*, 10th ed.; Molecular Probes: Eugene, OR, 2005.

- (6) Lavis, L. D. Teaching old dyes new tricks: Biological probes built from fluoresceins and rhodamines. *Annu. Rev. Biochem.* **2017**, *86*, 825–843.

- (7) Arden-Jacob, J.; Frantzeskos, J.; Kemnitzer, N. U.; Zilles, A.; Drexhage, K. H. New fluorescent markers for the red region. *Spectrochim. Acta, Part A* **2001**, *57*, 2271–2283.

- (8) Liu, J. X.; Diwu, Z. J.; Leung, W. Y.; Lu, Y. X.; Patch, B.; Haugland, R. P. Rational design and synthesis of a novel class of highly fluorescent rhodamine dyes that have strong absorption at long wavelengths. *Tetrahedron Lett.* **2003**, *44*, 4355–4359.

- (9) Kolmakov, K.; Belov, V.; Bierwagen, J.; Ringemann, C.; Mueller, V.; Eggeling, C.; Hell, S. Red-emitting rhodamine dyes for fluorescence microscopy and nanoscopy. *Chem. - Eur. J.* **2010**, *16*, 158–166.

- (10) Kolmakov, K.; Belov, V. N.; Wurm, C. A.; Harke, B.; Leutenegger, M.; Eggeling, C.; Hell, S. W. A versatile route to red-emitting carbopyronine dyes for optical microscopy and nanoscopy. *Eur. J. Org. Chem.* **2010**, *2010*, 3593–3610.

- (11) Koide, Y.; Urano, Y.; Hanaoka, K.; Terai, T.; Nagano, T. Evolution of Group 14 rhodamines as platforms for near-infrared fluorescence probes utilizing photoinduced electron transfer. *ACS Chem. Biol.* **2011**, *6*, 600–608.

- (12) Egawa, T.; Hanaoka, K.; Koide, Y.; Ujita, S.; Takahashi, N.; Ikegaya, Y.; Matsuki, N.; Terai, T.; Ueno, T.; Komatsu, T.; Nagano, T. Development of a far-red to near-infrared fluorescence probe for calcium ion and its application to multicolor neuronal imaging. *J. Am. Chem. Soc.* **2011**, *133*, 14157–14159.

- (13) Grimm, J. B.; Sung, A. J.; Legant, W. R.; Hulamm, P.; Matlosz, S. M.; Betzig, E.; Lavis, L. D. Carbofluoresceins and carborhodamines as scaffolds for high-contrast fluorogenic probes. *ACS Chem. Biol.* **2013**, *8*, 1303–1310.

- (14) Lukinavičius, G.; Umezawa, K.; Olivier, N.; Honigsmann, A.; Yang, G.; Plass, T.; Mueller, V.; Reymond, L.; Corrêa Jr, I. R.; Luo, Z. G.; Schultz, C.; Lemke, E. A.; Heppenstall, P.; Eggeling, C.; Manley, S.; Johnsson, K. A near-infrared fluorophore for live-cell super-resolution microscopy of cellular proteins. *Nat. Chem.* **2013**, *5*, 132–139.

- (15) Chai, X.; Cui, X.; Wang, B.; Yang, F.; Cai, Y.; Wu, Q.; Wang, T. Near-infrared phosphorus-substituted rhodamine with emission wavelength above 700 nm for bioimaging. *Chem. - Eur. J.* **2015**, *21*, 16754–16758.

- (16) Grimm, J. B.; English, B. P.; Chen, J.; Slaughter, J. P.; Zhang, Z.; Revyakin, A.; Patel, R.; Macklin, J. J.; Normanno, D.; Singer, R. H.; Lionnet, T.; Lavis, L. D. A general method to improve fluorophores for live-cell and single-molecule microscopy. *Nat. Methods* **2015**, *12*, 244–250.

- (17) Zhou, X.; Lai, R.; Beck, J. R.; Li, H.; Stains, C. I. Nebraska red: A phosphinate-based near-infrared fluorophore scaffold for chemical biology applications. *Chem. Commun.* **2016**, *52*, 12290–12293.

- (18) Liu, J.; Sun, Y.-Q.; Zhang, H.; Shi, H.; Shi, Y.; Guo, W. Sulfone-rhodamines: A new class of near-infrared fluorescent dyes for bioimaging. *ACS Appl. Mater. Interfaces* **2016**, *8*, 22953–22962.

- (19) Grimm, J. B.; Brown, T. A.; Tkachuk, A. N.; Lavis, L. D. General synthetic method for Si-fluoresceins and Si-rhodamines. *ACS Cent. Sci.* **2017**, *3*, 975–985.

- (20) Grimm, J. B.; Muthusamy, A. K.; Liang, Y.; Brown, T. A.; Lemon, W. C.; Patel, R.; Lu, R.; Macklin, J. J.; Keller, P. J.; Ji, N.; Lavis, L. D. A general method to fine-tune fluorophores for live-cell and in vivo imaging. *Nat. Methods* **2017**, *14*, 987–994.

- (21) Grimm, J. B.; Heckman, L. M.; Lavis, L. D. The chemistry of small-molecule fluorogenic probes. *Prog. Mol. Biol. Transl. Sci.* **2013**, *113*, 1–34.

- (22) Lukinavičius, G.; Reymond, L.; D'Este, E.; Masharina, A.; Gottfert, F.; Ta, H.; Guthrie, A.; Fournier, M.; Rizzo, S.; Waldmann, H.; Blaukopf, C.; Sommer, C.; Gerlich, D. W.; Arndt, H.-D.; Hell, S. W.

Johnsson, K. Fluorogenic probes for live-cell imaging of the cytoskeleton. *Nat. Methods* **2014**, *11*, 731–733.

(23) Lukinavičius, G.; Blaukopf, C.; Pershagen, E.; Schena, A.; Reymond, L.; Derivery, E.; Gonzalez-Gaitan, M.; D'Este, E.; Hell, S. W.; Wolfram Gerlich, D.; Johnsson, K. SiR–Hoechst is a far-red DNA stain for live-cell nanoscopy. *Nat. Commun.* **2015**, *6*, 8497.

(24) Lukinavičius, G.; Reymond, L.; Umezawa, K.; Sallin, O.; D'Este, E.; Gottfert, F.; Ta, H.; Hell, S. W.; Urano, Y.; Johnsson, K. Fluorogenic probes for multicolor imaging in living cells. *J. Am. Chem. Soc.* **2016**, *138*, 9365–9368.

(25) Li, X.; Gao, X.; Shi, W.; Ma, H. Design strategies for water-soluble small molecular chromogenic and fluorogenic probes. *Chem. Rev.* **2014**, *114*, 590–659.

(26) Spahn, C.; Grimm, J. B.; Lavis, L. D.; Lampe, M.; Heilemann, M. Whole-cell, 3D, and multicolor STED imaging with exchangeable fluorophores. *Nano Lett.* **2019**, *19*, 500–505.

(27) Reichardt, C. Solvatochromic dyes as solvent polarity indicators. *Chem. Rev.* **1994**, *94*, 2319–2358.

(28) Prifti, E.; Reymond, L.; Umezawa, M.; Hovius, R.; Riezman, H.; Johnsson, K. A fluorogenic probe for SNAP-tagged plasma membrane proteins based on the solvatochromic molecule Nile Red. *ACS Chem. Biol.* **2014**, *9*, 606–612.

(29) Lavis, L. D.; Rutkoski, T. J.; Raines, R. T. Tuning the pK_a of fluorescein to optimize binding assays. *Anal. Chem.* **2007**, *79*, 6775–6782.

(30) Han, J.; Burgess, K. Fluorescent indicators for intracellular pH. *Chem. Rev.* **2010**, *110*, 2709–2728.

(31) Shieh, P.; Dien, V. T.; Beahm, B. J.; Castellano, J. M.; Wyss-Coray, T.; Bertozzi, C. R. CalFluors: A universal motif for fluorogenic azide probes across the visible spectrum. *J. Am. Chem. Soc.* **2015**, *137*, 7145–7151.

(32) Sun, X.; Zhang, A.; Baker, B.; Sun, L.; Howard, A.; Buswell, J.; Maurel, D.; Masharina, A.; Johnsson, K.; Noren, C. J.; Xu, M.-Q.; Corrêa, I. R., Jr. Development of SNAP-tag fluorogenic probes for wash-free fluorescence imaging. *ChemBioChem* **2011**, *12*, 2217–2226.

(33) Brewer, T. F.; Chang, C. J. An azido-cope reactivity-based fluorescent probe for imaging formaldehyde in living cells. *J. Am. Chem. Soc.* **2015**, *137*, 10886–10889.

(34) Krishnamoorthy, L.; Cotruvo Jr, J. A.; Chan, J.; Kaluarachchi, H.; Muchenditsi, A.; Pendyala, V. S.; Jia, S.; Aron, A. T.; Ackerman, C. M.; Wal, M. N. V.; Guan, T.; Smaga, L. P.; Farhi, S. L.; New, E. J.; Lutsenko, S.; Chang, C. J. Copper regulates cyclic-AMP-dependent lipolysis. *Nat. Chem. Biol.* **2016**, *12*, 586–592.

(35) Uno, S.-n.; Kamiya, M.; Yoshihara, T.; Sugawara, K.; Okabe, K.; Tarhan, M. C.; Fujita, H.; Funatsu, T.; Okada, Y.; Tobita, S.; Urano, Y. A spontaneously blinking fluorophore based on intramolecular spirocyclization for live-cell super-resolution imaging. *Nat. Chem.* **2014**, *6*, 681–689.

(36) Fuguet, E.; Ràfols, C.; Rosés, M.; Bosch, E. Critical micelle concentration of surfactants in aqueous buffered and unbuffered systems. *Anal. Chim. Acta* **2005**, *548*, 95–100.

(37) Lukinavičius, G.; Mitronova, G. Y.; Schnorrenberg, S.; Butkevich, A. N.; Barthel, H.; Belov, V. N.; Hell, S. W. Fluorescent dyes and probes for super-resolution microscopy of microtubules and tracheoles in living cells and tissues. *Chem. Sci.* **2018**, *9*, 3324–3334.

(38) Deumié, M.; El Baraka, M. Self-aggregation of R110 and R123 rhodamines with surfactants and phospholipid vesicles of negative charge: A qualitative fluorescence study. *J. Photochem. Photobiol., A* **1993**, *74*, 255–266.

(39) Ferguson, J.; Mau, A. W. H. Absorption studies of acid-base equilibria of dye solutions. *Chem. Phys. Lett.* **1972**, *17*, 543–546.

(40) Hinkley, D. A.; Seybold, P. G. A spectroscopic/thermodynamic study of the rhodamine B lactone–zwitterion equilibrium. *Spectrochim. Acta, Part A* **1988**, *44*, 1053–1059.

(41) Nagano, T.; Hanaoka, K.; Koide, Y.; Egawa, T.; Kushida, Y. *Fluorescent probe*. U.S. Patent 9,329,184, 2016.

(42) Grimm, J. B.; Lavis, L. D. Synthesis of rhodamines from fluoresceins using Pd-catalyzed C–N cross-coupling. *Org. Lett.* **2011**, *13*, 6354–6357.

(43) Grimm, J. B.; English, B. P.; Choi, H.; Muthusamy, A. K.; Mehl, B. P.; Dong, P.; Brown, T. A.; Lippincott-Schwartz, J.; Liu, Z.; Lionnet, T.; Lavis, L. D. Bright photoactivatable fluorophores for single-molecule imaging. *Nat. Methods* **2016**, *13*, 985–988.

(44) Abdelfattah, A. S.; Kawashima, T.; Singh, A.; Novak, O.; Liu, H.; Shuai, Y.; Huang, Y.-C.; Campagnola, L.; Seeman, S. C.; Yu, J.; Zheng, J.; Grimm, J. B.; Patel, R.; Friedrich, J.; Mensh, B. D.; Paninski, L.; Macklin, J. J.; Murphy, G. J.; Podgorski, K.; Lin, B.-J.; Chen, T.-W.; Turner, G. C.; Liu, Z.; Koyama, M.; Svoboda, K.; Ahrens, M. B.; Lavis, L. D.; Schreier, E. R. Bright and photostable chemigenetic indicators for extended in vivo voltage imaging. *Science* **2019**, *365*, 699–704.

(45) Surry, D. S.; Buchwald, S. L. Dialkylbiaryl phosphines in Pd-catalyzed amination: A user's guide. *Chem. Sci.* **2011**, *2*, 27–50.

(46) Butkevich, A. N.; Bossi, M. L.; Lukinavičius, G.; Hell, S. W. Triarylmethane fluorophores resistant to oxidative photobleaching. *J. Am. Chem. Soc.* **2019**, *141*, 981–989.

(47) Miller, L. W.; Cai, Y.; Sheetz, M. P.; Cornish, V. W. In vivo protein labeling with trimethoprim conjugates: A flexible chemical tag. *Nat. Methods* **2005**, *2*, 255.

(48) Nakamura, A.; Takigawa, K.; Kurishita, Y.; Kuwata, K.; Ishida, M.; Shimoda, Y.; Hamachi, I.; Tsukiji, S. Hoechst tagging: A modular strategy to design synthetic fluorescent probes for live-cell nucleus imaging. *Chem. Commun.* **2014**, *50*, 6149–6152.

(49) Legant, W. R.; Shao, L.; Grimm, J. B.; Brown, T. A.; Milkie, D. E.; Avants, B. B.; Lavis, L. D.; Betzig, E. High-density three-dimensional localization microscopy across large volumes. *Nat. Methods* **2016**, *13*, 359–365.

(50) Shao, L.; Kner, P.; Rego, E. H.; Gustafsson, M. G. Super-resolution 3D microscopy of live whole cells using structured illumination. *Nat. Methods* **2011**, *8*, 1044–1046.

(51) Klar, T. A.; Jakobs, S.; Dyba, M.; Egner, A.; Hell, S. W. Fluorescence microscopy with diffraction resolution barrier broken by stimulated emission. *Proc. Natl. Acad. Sci. U. S. A.* **2000**, *97*, 8206–8210.

(52) Chen, B.-C.; Legant, W. R.; Wang, K.; Shao, L.; Milkie, D. E.; Davidson, M. W.; Janetopoulos, C.; Wu, X. S.; Hammer, J. A.; Liu, Z.; English, B. P.; Mimori-Kiyosue, Y.; Romero, D. P.; Ritter, A. T.; Lippincott-Schwartz, J.; Fritz-Laylin, L.; Mullins, R. D.; Mitchell, D. M.; Bembek, J. N.; Reymann, A.-C.; Böhme, R.; Grill, S. W.; Wang, J. T.; Seydoux, G.; Tulu, U. S.; Kiehart, D. P.; Betzig, E. Lattice light-sheet microscopy: Imaging molecules to embryos at high spatiotemporal resolution. *Science* **2014**, *346*, 1257998.

(53) Takakura, H.; Zhang, Y.; Erdmann, R. S.; Thompson, A. D.; Lin, Y.; McNellis, B.; Rivera-Molina, F.; Uno, S.-n.; Kamiya, M.; Urano, Y.; Rothman, J. E.; Bewersdorf, J.; Schepartz, A.; Toomre, D. Long time-lapse nanoscopy with spontaneously blinking membrane probes. *Nat. Biotechnol.* **2017**, *35*, 773–780.

(54) Jradi, F. M.; Lavis, L. D. Chemistry of photosensitive fluorophores for single-molecule localization microscopy. *ACS Chem. Biol.* **2019**, *14*, 1077–1090.

(55) Banfi, L.; Narisano, E.; Riva, R. In *Handbook of reagents for organic synthesis: Oxidizing and reducing agents*; Burke, S. D., Danheiser, R. L., Eds.; John Wiley and Sons: New York, 1999; pp 209–212.

(56) Whitaker, J. E.; Haugland, R. P.; Ryan, D.; Hewitt, P. C.; Haugland, R. P.; Prendergast, F. G. Fluorescent rhodol derivatives: Versatile, photostable labels and tracers. *Anal. Biochem.* **1992**, *207*, 267–279.

(57) Sednev, M. V.; Wurm, C. A.; Belov, V. N.; Hell, S. W. Carborhodol: A new hybrid fluorophore obtained by combination of fluorescein and carbopyronine dye cores. *Bioconjugate Chem.* **2013**, *24*, 690–700.

(58) Fang, Y.; Good, G. N.; Zhou, X.; Stains, C. I. Phosphinate-containing rhodol and fluorescein scaffolds for the development of bioprobes. *Chem. Commun.* **2019**, *55*, 5962–5965.

(59) Enander, K.; Choulier, L.; Olsson, A. L.; Yushchenko, D. A.; Kanmert, D.; Klymchenko, A. S.; Demchenko, A. P.; Mély, Y.; Altschuh, D. A peptide-based, ratiometric biosensor construct for direct fluorescence detection of a protein analyte. *Bioconjugate Chem.* **2008**, *19*, 1864–1870.

(60) Deo, C.; Lavis, L. D. Synthetic and genetically encoded fluorescent neural activity indicators. *Curr. Opin. Neurobiol.* **2018**, *50*, 101–108.

(61) MacNevin, C. J.; Watanabe, T.; Weitzman, M.; Gulyani, A.; Fuehrer, S.; Pinkin, N. K.; Tian, X.; Liu, F.; Jin, J.; Hahn, K. M. Membrane-permeant, environment-sensitive dyes generate biosensors within living cells. *J. Am. Chem. Soc.* **2019**, *141*, 7275–7282.